Available online at www.sciencedirect.com
ScienceDirect
Trans. Nonferrous Met. Soc. China 25(2015) 4028−4039
Transactions of Nonferrous Metals Society of China
www.tnmsc.cn

In vitro corrosion and antibacterial properties of layer-by-layer assembled GS/PSS coating on AZ31 magnesium alloys

Rong-chang ZENG[1,2], Li-jun LIU[1], Kai-jie LUO[1], Li SHEN[1], Fen ZHANG[1], Shuo-qi LI[1], Yu-hong ZOU[3]

1. College of Materials Science and Engineering, Shandong University of Science and Technology, Qingdao 266590, China;
2. State Key Laboratory of Mining Disaster Prevention and Control Co-founded by Shandong Province and the Ministry of Science and Technology, Shandong University of Science and Technology, Qingdao 266590, China;
3. College of Chemical and Environmental Engineering, Shandong University of Science and Technology, Qingdao 266590, China

Received 24 January 2015; accepted 10 June 2015

Abstract: To enhance the corrosion resistance of magnesium (Mg) alloy and to impart its surface with antibacterial functionality for inhibiting biofilm formation and biocorrosion, $Mg(OH)_2$ films were fabricated on AZ31 magnesium alloy substrates by an in-situ hydrothermal method and well-defined multilayer coatings, consisting of gentamicin sulfate (GS) and poly(sodium 4-styrene sulfonate) (PSS), were prepared via layer-by-layer (LbL) assembly. The morphologies, chemical compositions and corrosion resistance of the obtained $(PSS/GS)_n$/Mg sample were investigated using scanning electron microscopy, Fourier transform infrared spectroscopy, X-ray photoelectron spectroscopy, electrochemical methods and immersion tests. Finally, the bactericidal activity of $(PSS/GS)_n$/Mg samples against *Staphylococcus aureus* was assessed by the zone of inhibition methods and plate-counting method. The so-synthesized composite coating on the Mg alloy substrates exhibits good corrosion resistance and antibacterial performance, which make them attractive as coatings for medical implanted devices.

Key words: magnesium alloy; corrosion resistance; antibacterial property; layer-by-layer assembly

1 Introduction

Magnesium alloys have been intensively investigated as potential candidates for orthopedic and cardiovascular stent applications owing to their good biocompatibility, unique biodegradability and better mechanical properties compared with the other types of biodegradable materials such as polymer and ceramic [1−5]. However, a relatively poor resistance to corrosion is a serious impediment against wider application of magnesium alloys [6,7]. Therefore, some methods must be supplied to improve the corrosion resistance of magnesium and its alloys [8,9]. One of the most significant ways to protect corrosion is to coat the base materials.

On the other hand, while issues related to rapid surface degradation must be solved, good antibacterial properties are also necessary. The biomaterials as implants were believed to be at the risk of the adsorption of bacteria and the subsequent bacterial colonization and biofilm formation on the surfaces when exposed to the living tissue. Afterward, infections are usually caused by the bacterial adhering and colonizing on implants and then lead to the development of a biofilm, which would damage surrounding tissues and generate planktonic bacterial cells that spread infection [10]. Therefore, antibacterial properties play a significant role in determining the outcome and success of an implant [11,12] and it is highly desirable to fabricate a new class of coating on Mg alloys to reduce the corrosion rate while concomitantly suppressing the proliferation of the bacterial.

Among the various technologies available for

Foundation item: Project (2014TDJH104) supported by Shandong University of Science and Technology (SDUST) Research Fund, China; Project (2013RCJJ006) supported by Scientific Research Foundation of Shandong University of Science and Technology for Recruited Talents, China; Project (BS2013CL009) supported by Scientific Research Foundation of Shandong for Outstanding Young Scientist, China
Corresponding author: Shuo-qi LI; Tel: +86-532-86051385; E-mail: lishuoqi@sdust.edu.cn
DOI: 10.1016/S1003-6326(15)64052-3

coating, the process known as layer-by-layer (LbL) self-assembly, is a simple, versatile, and inexpensive approach to generate functional multilayer thin coatings on surface [13,14]. By incubating a substrate in alternating solutions of positively and negatively charged polyelectrolyte, thin well-adhered film layers are formed as expected [15]. Some researches show that the advantages of the LbL self-assembly of polyelectrolytes on metal are that they do not contain toxic and harmful substances and the production process is simple and economical [16]. LbL self-assembly films have been utilized as drug carrier systems to reduce the possibility of localized infection. For instance, SCHMIDT et al [17] reported an LbL film composed primarily of nanoparticles and small molecules, demonstrating a systematic electro-activated drug release from such films. MIN et al [18] developed a multi-agent delivery thin LbL film with controlled local release of gentamicin.

In this work, the coated AZ31 substrates were prepared by hydrothermal treatment with NaOH solution and electrostatic-based LbL self-assembly. The obtained $Mg(OH)_2$ film as an inner layer has been used in order to enhance the corrosion resistance because it works as a barrier between the substrate and body fluids [19]. The assembled films are composed of poly(styrene sulfonate) (PSS) and a small molecule antibiotic, gentamicin sulfate (GS), which is an aminoglycoside antibiotic, for use in the treatment of severe infections caused by both Gram-positive and, especially, Gram-negative bacteria [20,21]. GS serves as the cationic component of the LbL film and PSS is the anionic component. To our knowledge, there were few reports about functional composite films combining corrosion resistance and antibacterial properties on magnesium alloy. The physicochemical properties of the composite films were characterized using different analytical techniques. Furthermore, the effects of LbL films on the corrosion and bactericidal efficiency against *Staphylococcus aureus* (*S. aureus*) were studied.

2 Experimental

2.1 Materials and chemicals

The as-extruded AZ31 magnesium alloy used has nominal chemical composition (mass fraction, %): Al 2.5−3.0, Zn 0.7−1.3, Mn>0.20 and balanced Mg. PSS (M_r=70000) and polyethyleneimine (PEI, M_r=600) were purchased from Qingdao Jingke Chemical Reagent Co., Ltd., China. GS (M_r=575.67) was purchased from Chengdu Ai Ke Chemical Technology Co., Ltd., China. Figure 1 shows the chemical structures of PSS and GS used in this work. All chemicals were of analytical grade and deionized (DI) water was used throughout to prepare the solutions and wash the samples.

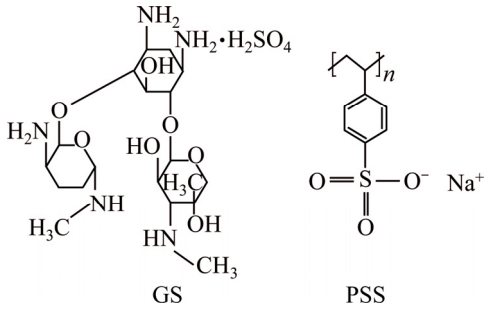

Fig. 1 Chemical structures of GS and PSS

2.2 Preparation of composite coatings

The substrates with dimensions of 20 mm × 20 mm × 3 mm were polished with SiC papers up to 1500 grit, washed with DI water to remove excess impurities and dried in air. A hydrothermal method was utilized to treat the prepared Mg alloy. In brief, sodium hydroxide (10 g) was added into DI water (100 mL) with stirring. Then, the solution and the substrates were transferred into a 100 mL Teflon-lined stainless. The autoclave was kept in an electric oven at 170 °C for 3 h. Finally, the substrates were washed thoroughly with DI water several times and dried in air [22,23]. The samples prepared under this process were denoted as NaOH-treated Mg.

Layer-by-layer coatings were created via a dip-coating method, wherein the NaOH-treated Mg samples were firstly immersed in the PEI solution (10 mg/mL) for 10 min to obtain a precursor layer with a stable positive charge to initiate the LbL assembly process [24,25]. Then, the layers were generated with the following sequence: BCBCBCBCB (B and C represent negatively and positively charged polyelectrolytes, respectively). Solutions B and C contain anionic polyelectrolyte, PSS (pH=5.5) at 2 mg/mL and GS (pH=5.5) at 2 mg/mL. Thus, each bilayer consists of PSS layer and GS layer. The dipping cycles were repeated until $(PSS/GS)_n$/Mg (where n denotes the number of bilayers) samples were obtained. Figure 2 outlines the idealized pictures of the proposed methodology schematically.

2.3 Surface characterization

The surface morphologies of the coatings were observed by means of scanning electron microscopy (SEM, Nova NanoSem 450) equipped with energy-dispersive X-ray spectroscopy (EDS). The possible chemical bonding formed in the coatings was confirmed by Fourier transform infrared spectrometry (FTIR, Nicolet 380, Thermo Electron Corporation) and X-ray photoelectron spectroscopy (XPS, ESCALAB250, Thermo VG Corporation). For the FTIR measurements,

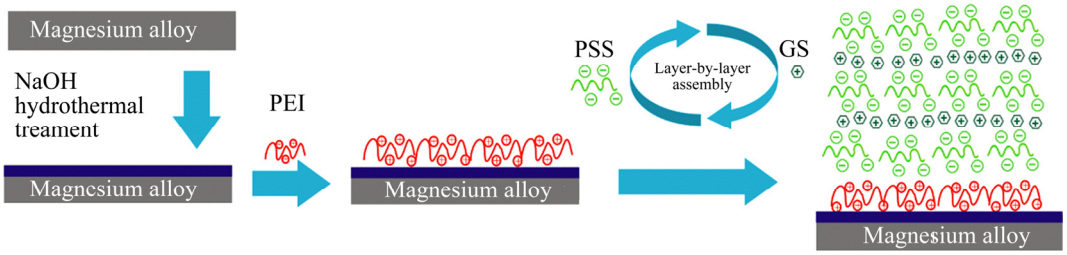

Fig. 2 Schematic representation of construction of $(PSS/GS)_n$/Mg samples

the multilayered components carefully taken from the samples were diluted in KBr (0.2%, mass fraction) to generate pellets and were analyzed in the absorbance mode using a resolution of 4 cm^{-1} and a total of 32 scans.

2.4 Electrochemical measurements and hydrogen evolution

The potentiodynamic polarization curves and electrochemical impedance spectroscopy (EIS) were performed by an electrochemical analyzer (PAR Model 2273, Princeton). A three-electrode cell set-up was used wherein the prepared coated AZ31 alloy samples, saturated calomel electrode (SCE) and a platinum wire were used as the working, reference and counter electrodes, respectively. The polarization curves were tested at a constant scan rate of 2 mV/s, initiated from −2000 mV to −1000 mV. EIS studies were carried out at open circuit potential for 10 mV sinusoidal amplitude over a frequency range of 100 kHz to 0.01 Hz. A stable open circuit potential was established prior to testing. All experiments were conducted at room temperature in simulated body fluid (SBF) with a pH of 7.40. The chemical composition of the SBF is listed in Table 1. Each test was duplicated to prove the reproducibility of the results.

Table 1 Chemical composition of SBF

Reagent	ρ/(g·L^{-1})
NaCl	8.035
$NaHCO_3$	0.335
KCl	0.225
$KH_2PO_4·3H_2O$	0.231
$MgCl_2·6H_2O$	0.423
$CaCl_2$	0.292
Na_2SO_4	0.072
Tris [a]	6.228

[a] Tris = 2-amino-2-(hydroxymethyl)-1,3-propanediol

The hydrogen evolution set-up design was tested by placing the sample with full surface exposure in SBF at 37 °C under an inverted funnel connected to a graduated burette. The water level in the burette was intermittently recorded during the immersion experiment for 9 d. The hydrogen evolution rate (HER) can be calculated by [26]

$$HER=V_H/st \quad (1)$$

where V_H is the hydrogen evolution volume, s is the exposed area and t is the immersion time.

2.5 Antibacterial assays

The antibacterial spectrum of the samples was evaluated by zone of inhibition (ZOI) testing. Gram-positive *Staphylococcus aureus* (*S. aureus*) was cultured in agar plates at 37 °C overnight. The optical density of the test organism was adjusted to 0.699 at 650 nm, which indicated the content of bacteria approximately reached 10^9 colony-forming units (CFU)/mL. Freshly grown bacteria were diluted by broth to an approximate concentration of 5×10^7 CFU/mL of *S. aureus*. 10 mL of this stock solution was spread onto the surface of an agar plate. The Mg, NaOH-treated Mg, $(PSS/GS)_{20}$/Mg and $(PSS/GS)_{60}$/Mg samples were placed on the inoculated agar plates and incubated at 37 °C for 24 h. Colonies were visualized and images of the clear zones around the samples were captured [27].

To further investigate the antibacterial effects of the coated Mg alloy, the plate-counting method was used [28]. The sample was added to 3 mL of broth containing approximately 10^6 CFU/mL of *S. aureus*. After 2 h of treatment, the suspension was diluted with 0.8% NaCl solution, and then approximately 1.8×10^3 CFU of *S. aureus* was swabbed onto an agar plate. The plate was then incubated at 37 °C for 16 h. The colonies were then counted to evaluate bactericidal activity of the PSS/GS modified Mg by comparison with the native Mg alloy.

3 Results and discussion

3.1 SEM images of composite film on substrate

The surface morphologies of the bare and coated Mg alloy were examined using SEM and are shown in Fig. 3. The surfaces of bare AZ31 alloy (Fig. 3(a)) and NaOH-treated Mg (Fig. 3(b)) display similar morphology and the scratches on the surface are less obvious after hydrothermal treatment. The SEM images of $(PSS/GS)_{20}$/Mg (Fig. 3(c)) and $(PSS/GS)_{60}$/Mg (Fig. 3(d)) show that

the surfaces are covered by polyelectrolyte coatings after the modification by PSS/GS bilayers. However, some defects are presented on the surfaces and when the bilayers number is increased, more defects are observed, which may be ascribed to the fact that the AlMnSi [29] particles are preferentially corroded due to the interaction between the $Mg(OH)_2$ film matrix and the assembled units. This is responsible for the reduction in corrosion protection on Mg alloy in SBF solution.

The cross-sectional morphologies of the samples are shown in Fig. 4. The total thicknesses of different coatings are 14.5, 9.6 and 5.4 μm for the NaOH-treated Mg, $(PSS/GS)_{20}$/Mg and $(PSS/GS)_{60}$/Mg samples, respectively. The distinction in thickness is engendered by different number of the assembled layers, which can be ascribed to the fact that the LbL process would decrease the thickness of the $Mg(OH)_2$ film. It has been reported that the protection provided by coatings is proportional to the coating thickness [30], thus the assembly would result in a low corrosion resistance of the sample.

3.2 FTIR spectra

FTIR testing has been used to validate the development of the composite coatings on the AZ31 substrates. As can be seen in Fig. 5, all the samples show the stretching vibration bands for hydroxyl group (3695 cm^{-1}) and Mg—O (447 cm^{-1}) of $Mg(OH)_2$ [31,32].

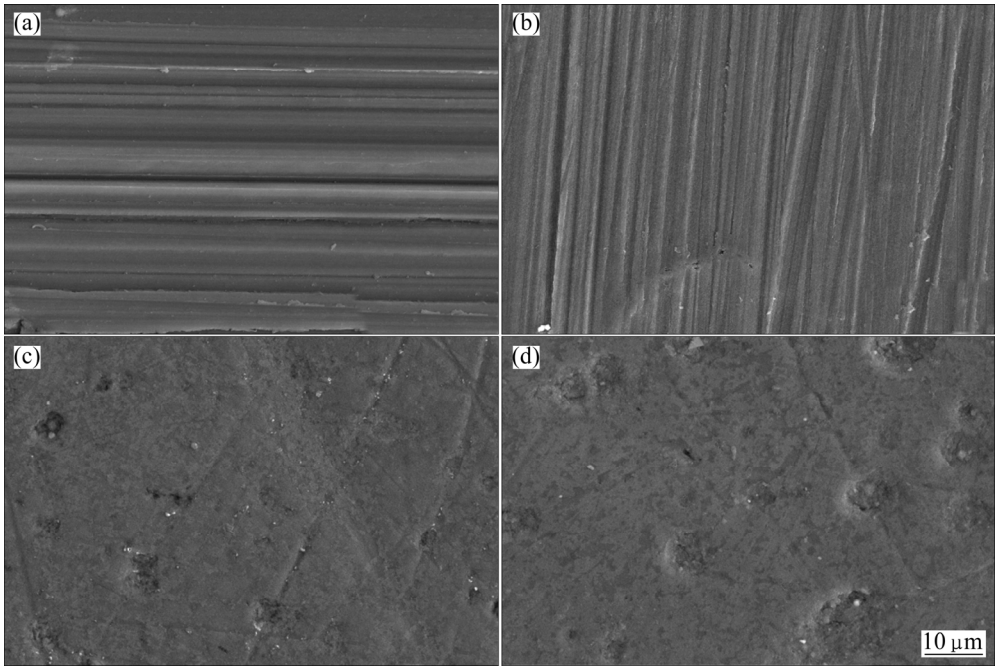

Fig. 3 SEM images of surfaces of Mg alloy (a), NaOH-treated Mg (b), $(PSS/GS)_{20}$/Mg (c) and $(PSS/GS)_{60}$/Mg (d) samples

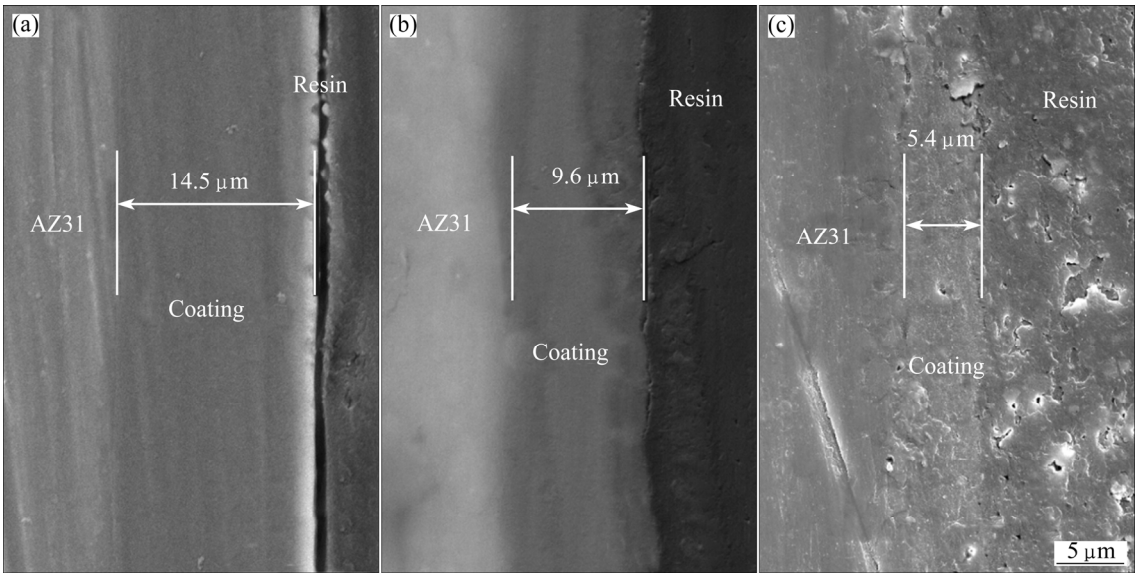

Fig. 4 Cross-sectional SEM images of NaOH-treated Mg (a), $(PSS/GS)_{20}$/Mg (b) and $(PSS/GS)_{60}$/Mg (c) samples

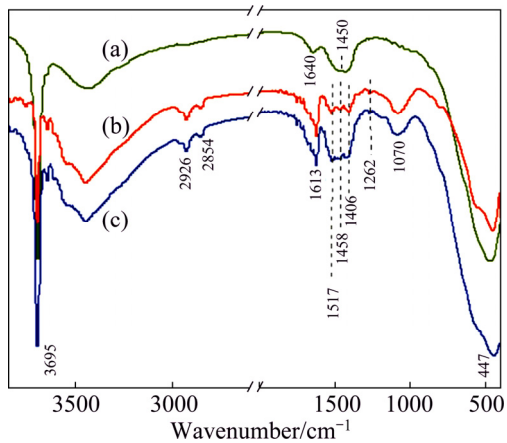

Fig. 5 FTIR absorption spectra of prepared NaOH-treated Mg (a), $(PSS/GS)_{20}$/Mg (b) and $(PSS/GS)_{60}$/Mg (c)

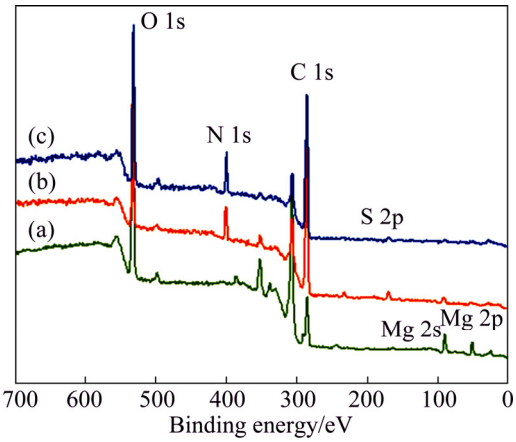

Fig. 6 XPS spectra of NaOH-treated Mg (a), $(PSS/GS)_{20}$/Mg (b) and $(PSS/GS)_{60}$/Mg (c)

As for the NaOH-treated Mg, the bands at 1640 cm^{-1} arises from H_2O bending vibration and the band for carbonate group is observed at 1450 cm^{-1} [33]. After the modification of PSS/GS, the FTIR spectra (curves (b) and (c)) show peaks at 2926 and 2854 cm^{-1} that are attributed to stretching vibrations of —CH and —CH_2 groups from the assembled multilayer [34]. Notably, the band at 1613 cm^{-1} is assigned to the stretching vibration of C═C groups of PSS [35] and the two bands at 1262 and 1070 cm^{-1} are assigned to the asymmetric and symmetric vibrations of the —SO_3H groups of PSS [34], respectively. Meanwhile, the absorption bands at 1517, 1458 and 1406 cm^{-1} are related to the bending of N—H bond of the primary and secondary amines, which are the characteristic groups of GS [36]. All these absorptions confirm a successful construction of the PSS/GS films. In addition, with the increase in the number of bilayers, the N—H adsorption peaks of GS increase, which suggests that more GS is assembled on the substrate.

3.3 XPS spectra

The XPS wide scan spectra of the samples were also employed to characterize the LbL process. As shown in Fig. 6, the spectrum of the NaOH-treated Mg displays the predominant elements of C, O and Mg, which indicates the formation of $Mg(OH)_2$ film. The high content of carbon is derived from the environmental contamination [37]. Successful PSS/GS modification on the surface of $Mg(OH)_2$ film was confirmed by the presence of additional peaks of N and S (curves (b) and (c)). Moreover, the N content is 6.44% for $(PSS/GS)_{20}$/Mg (curve (b)) and 8.4% for $(PSS/GS)_{60}$/Mg (curve (c)). This result shows that more GS could be immobilized on the substrate by increasing the number of the assembled bilayers, which is consistent with the conclusion from FTIR spectra.

3.4 Corrosion characterization

Polarization curves for the bare and coated substrates can be seen in Fig. 7. Table 2 gives a summary of the corrosion potential (φ_{corr}) and corrosion current density (J_{corr}) as calculated from extrapolation of the Tafel plots. All three coated samples, NaOH-treated Mg (curve (b)), $(PSS/GS)_{20}$/Mg (curve (c)) and $(PSS/GS)_{60}$/Mg (curve (d)) show lower J_{corr} values than the AZ31 alloy substrate (curve (a)), and the φ_{corr} values are more anodic than that of the bare AZ31 alloy. The NaOH treatment offers the greatest reduction in J_{corr} value, which is measured at 3.11×10^{-8} A/cm^2. This can be ascribed to the $Mg(OH)_2$ film retarding the penetration of species (such as water and chlorine) [38]. Nevertheless, the J_{corr} values of the $(PSS/GS)_{20}$/Mg and $(PSS/GS)_{60}$/Mg samples are 1.52×10^{-7} A/cm^2 and 6.11×10^{-6} A/cm^2, respectively, which show an increase in J_{corr} compared with that of the NaOH-treated Mg. Moreover, large number of assembled bilayers leads to a higher corrosion rate. This result can be ascribed to the fact that some

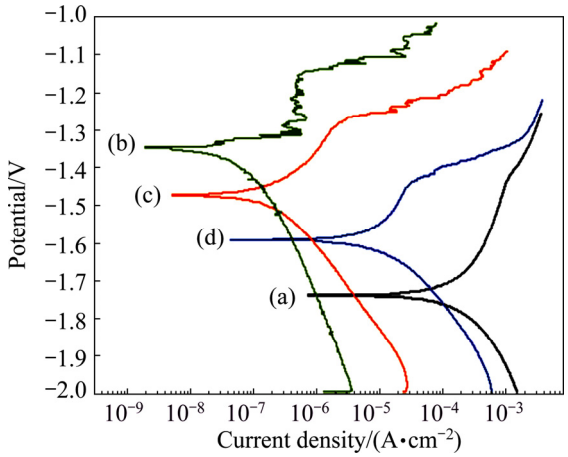

Fig. 7 Polarization curves of AZ31 alloy (a), NaOH-treated Mg (b), $(PSS/GS)_{20}$/Mg (c) and $(PSS/GS)_{60}$/Mg (d) immersed in SBF solution

Table 2 Electrochemical parameters of polarization curves

Sample	φ_{corr}/V	J_{corr}/(A·cm^{-2})
AZ31 alloy	−1.73	1.21×10^{-4}
NaOH-treated Mg	−1.33	3.11×10^{-8}
$(PSS/GS)_{20}$/Mg	−1.47	1.52×10^{-7}
$(PSS/GS)_{60}$/Mg	−1.59	6.11×10^{-6}

defects might be generated and the thickness of $Mg(OH)_2$ film would be decreased during the LbL assembly process [13,39]. Thus, the more the layers that are performed on the substrate, the larger the decline in the corrosion resistance of the sample. This result is consistent with the discussion in Section 3.1. However, even in this case, the J_{corr} values of the $(PSS/GS)_{20}$/Mg and $(PSS/GS)_{60}$/Mg samples are still lower than that of the bare AZ31 alloy, which demonstrates that the obtained samples have better anti-corrosive properties than the bare Mg substrate.

To further investigate the characteristics of the corrosion inhibition effect of the composite coating, EIS was employed in this study. Figure 8 shows the Nyquist and Bode plots of the bare and coated AZ31 alloy immersed in SBF solution. It is generally acknowledged that the diameter of the capacitive loop in Nyquist plots represents the polarization resistance of the working electrode [40]. The impedance values at the onset of immersion are 145 Ω·cm^2 for AZ31 alloy, 400 kΩ·cm^2 for NaOH-treated Mg, 140 kΩ·cm^2 for $(PSS/GS)_{20}$/Mg and 1900 Ω·cm^2 for $(PSS/GS)_{60}$/Mg, respectively. Thus, the Nyquist plots demonstrate that the corrosion resistance of the four samples reduces in the order of NaOH-treated Mg > $(PSS/GS)_{20}$/Mg > $(PSS/GS)_{60}$/Mg > AZ31 alloy, which is in agreement with the polarization curve results, indicating the better anticorrosion performance of composite coatings than the AZ31 substrate.

In addition, the Nyquist plots for the AZ31 alloy (Fig. 8(a)) are characterized by three loops: a high frequency (HF) capacitive loop, a medium frequency (MF) capacitive loop and a low frequency (LF) inductive loop, which is taken as an indication of pitting corrosion [41,42]. Thus, the corrosion of AZ31 alloy has begun in the initial stage of immersion. It is well known that higher impedance modulus $|Z|$ at lower frequency exhibits better corrosion resistance of the samples [43]. With increasing the immersion time to 2−8 h, the $|Z|$ values increase gradually, but reduce suddenly after immersion for 12 h, and then increase again after 24 h.

For the NaOH-treated Mg, the Nyquist plots (Fig. 8(c)) show two capacitive loops for 0−8 h of immersion. When the immersion time is increased to 12 h, the capacitive loop at MF disappears and an inductive loop shows up at low frequency, indicating the pitting corrosion. From the bode plots (Fig. 8(d)), the $|Z|$ values decease gradually as time evolves, suggesting that the $Mg(OH)_2$ film is degraded unceasingly.

The Nyquist plots for the $(PSS/GS)_{20}$/Mg (Fig. 8(e)) consist of two capacitive loops for 0−4 h of immersion. When the time is increased to 8 h, the capacitive loop gets much smaller and one inductive loop appears at the LF, indicating the dissolution of the composite coatings and the inducement of pitting on the substrate. As can be seen from the bode plots (Fig. 8(f)), the $|Z|$ values decease continuously for 8 h and increase slightly after 12 h. When the sample is immersed in SBF solution for 24 h, the $|Z|$ values decrease again.

When the sample is modified by 60 bilayers of PSS/GS, the Nyquist plots (Fig. 8(g)) show two capacitive loops at HF and MF and one inductive loop at LF, which demonstrates that the pitting corrosion has begun at the onset of immersion for $(PSS/GS)_{60}$/Mg samples. The bode plots show that the $|Z|$ values decease gradually for 8 h and increase slightly after 12 h immersion, then decrease again. The comparison of the overall impedance of the different coatings also indicates that the multilayer coating has higher protective ability than the bare Mg substrate and the protective property comes from the $Mg(OH)_2$ film, which is consistent with the SEM and Tafel measurements.

Alternatively, the corrosion rates of the samples were also assessed by hydrogen evolution. As presented in Fig. 9, the hydrogen evolution rate (HER) of the AZ31 substrate consistently decreases with time, whereas the HER of NaOH-treated Mg increases continuously in the first 30 h and descends successively and slowly. As for the PSS/GS modified samples, the HERs decrease with time during the initial stage, then dramatically rise to higher values and tend to decrease and stabilize in the subsequent stage.

Once immersed in corrosive solutions, the AZ31 alloys are corroded according to the following electrochemical reactions:

$$Mg \rightarrow Mg^{2+}+2e \quad (2)$$

$$2H_2O+2e \rightarrow 2OH^-+H_2 \quad (3)$$

The by-product (OH^-) of magnesium dissolution can raise localized corrosion and stabilize the corrosion product ($Mg(OH)_2$):

$$Mg^{2+}+2OH^- \rightarrow Mg(OH)_2 \quad (4)$$

As immersion proceeds, the thickness of the corrosion product layer increases and the corrosion rate decreases gradually [44]. When equilibrium between dissolution and formation of corrosion products is established, the corrosion rate stabilizes. In contrast with the AZ31 substrate, the HER of the NaOH-treated Mg increases in the first 30 h. Because when immersed in the

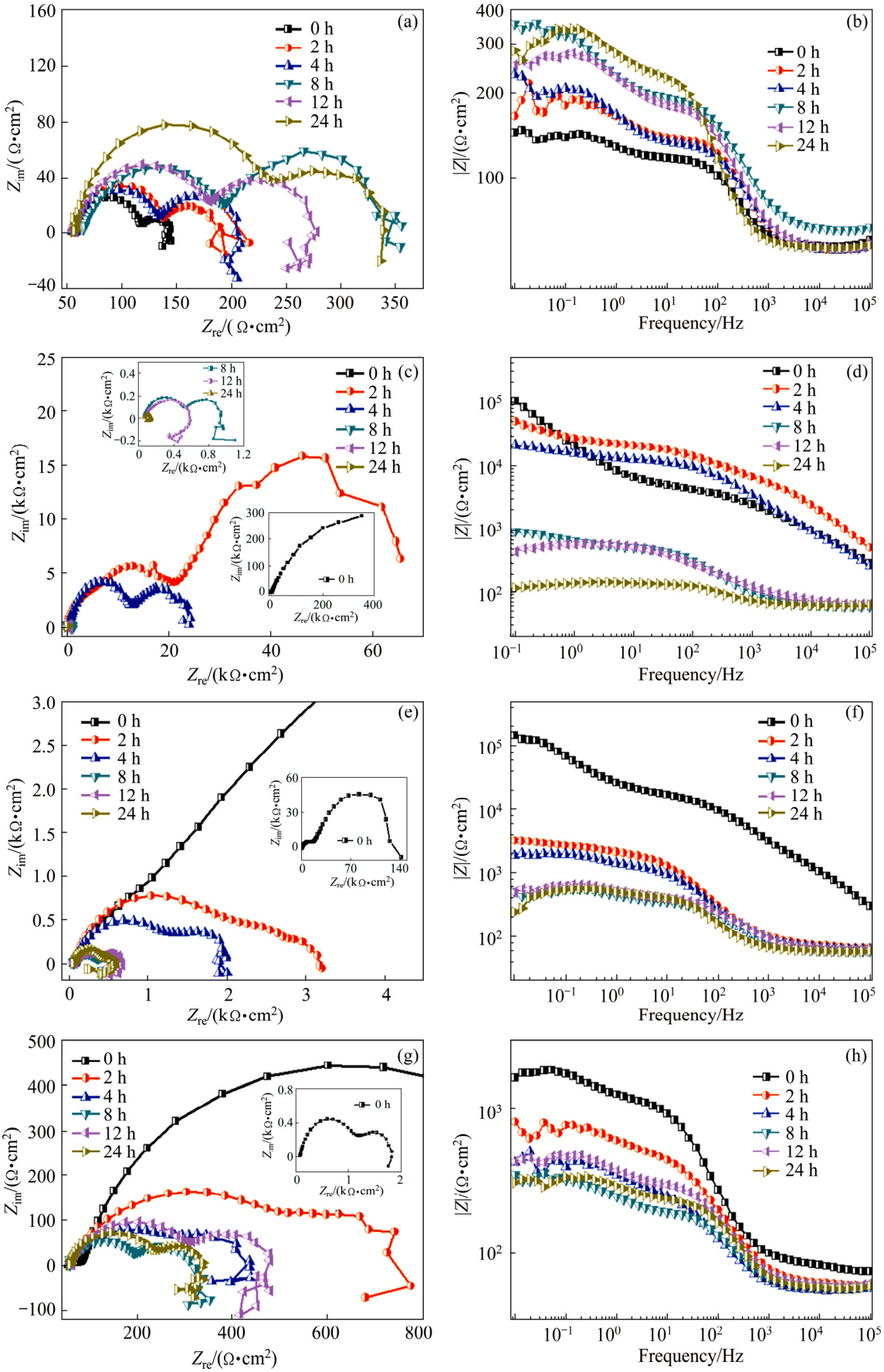

Fig. 8 Nyquist plots (a, c, e, g) and Bode diagrams (b, d, f, h) for AZ31 alloy (a, b), NaOH-treated Mg (c, d), $(PSS/GS)_{20}$/Mg (e, f) and $(PSS/GS)_{60}$/Mg (g, h) immersed in SBF solution

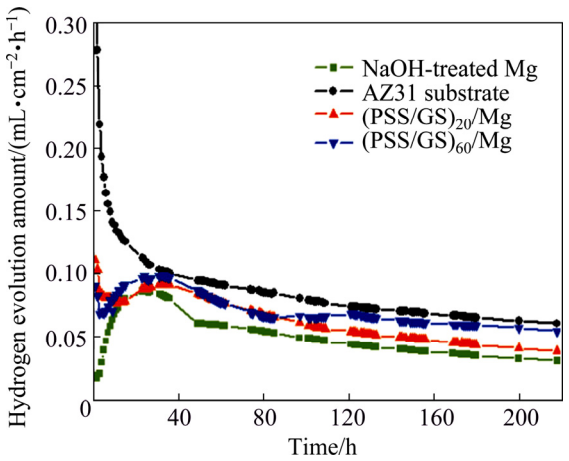

Fig. 9 Hydrogen evolution rates of AZ31 substrate and composite coatings immersed in SBF solution as function of immersion time

SBF solution, the $Mg(OH)_2$ film is attacked by chloride ions and transformed into $MgCl_2$. Dissolution of $Mg(OH)_2$ makes the surface more active, subsequently decreasing the protected area and resulting in an increase of the corrosion rate. Afterward, the corrosion products cover the surfaces and the degradation rate is nearly constant over time, which is about half that of AZ31 alloy. With the propulsion of assembly process, the HERs decrease rapidly in the first 4 h because of the protection of the multilayer coatings. When the corrosive medium penetrates into the $Mg(OH)_2$ film through the defects on the surfaces, the HERs continuously increase for sever hours. Finally, the HERs trends are similar to that of the NaOH-treated Mg.

On the whole, the corrosion rates of different samples follow the order of NaOH-treated Mg < $(PSS/GS)_{20}$/Mg < $(PSS/GS)_{60}$/Mg < AZ31 substrate. The trends are very much in agreement with the results observed by polarization measurements, which also indicates that the corrosion resistance of Mg alloy has been effectively improved after hydrothermal treatment and LbL assembly.

3.5 Morphology observation after immersion test

Figure 10 shows comparative optical macro-morphologies of samples after 9 d of immersion. Figures 10(a) and (b) show the morphologies of the AZ31 substrate and NaOH-treated Mg, and Figs. 10(c) and (d) illustrate those of the samples modified with 20 and 60 bilayers of PSS/GS, respectively. As can be seen, the corrosion area of the AZ31 substrate accounts for the great proportion of the surface, especially some edges are corroded severely. But for the NaOH-treated Mg, both area and depth of the local corrosion reduce significantly. From the magnitude of the corroded zone, it is clear that corrosion resistance of PSS/GS bilayers modified Mg alloy becomes weaker than that of the NaOH-treated Mg, and the more the number of bilayers is, the weaker the corrosion resistance is. However, the corrosion areas of $(PSS/GS)_{20}$/Mg and $(PSS/GS)_{60}$/Mg are still less than that the AZ31 substrate.

To investigate the microstructure evolutions of different samples after immersion, SEM measurements were performed (Fig. 11). Discernable crevices and randomly distributed deep pits along with white precipitates are observed on the surface of AZ31 substrate. For the NaOH-treated Mg, some cracks appear on the surface as a result of the dehydration of the layer during the drying process and the micro-pores are observed at high magnification. For the $(PSS/GS)_{20}$/Mg, some cracks and white particles in the cauliflower shape are formed on the surface, whereas rough morphology with deep pitting corrosion on the $(PSS/GS)_{60}$/Mg surface is observed. The EDS analysis results suggest

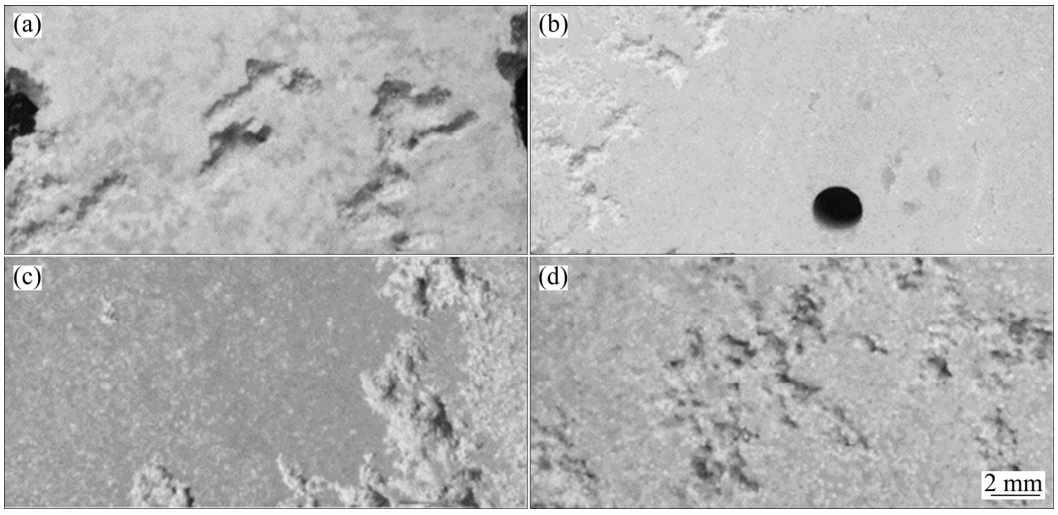

Fig. 10 Optical macro-morphologies of samples after being immersed in SBF solutions for 9 d: (a) AZ31 substrate; (b) NaOH-treated Mg; (c) $(PSS/GS)_{20}$/Mg; (d) $(PSS/GS)_{60}$/Mg

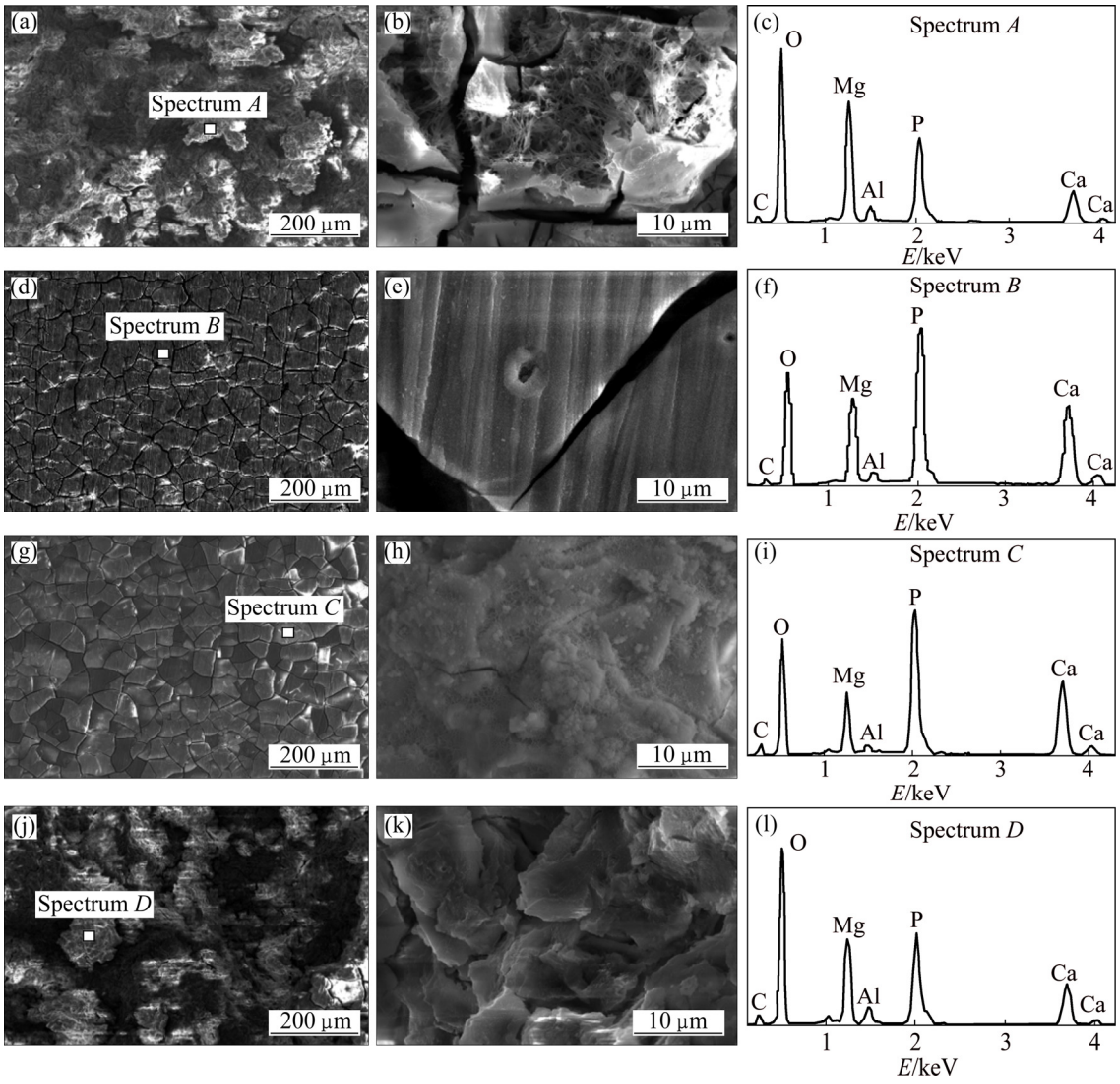

Fig. 11 SEM images of AZ31 substrate (a, b), NaOH-treated Mg (d, e), $(PSS/GS)_{20}$/Mg (g, h), $(PSS/GS)_{60}$/Mg (j, k) after immersion in SBF and corresponding EDS spectra of Spectrum *A* (c), spectrum *B* (f), spectrum *C* (i) and spectrum *D* (l)

that the surface degradation products of the samples are rich in O, Mg, P and Ca. This indicates that P and Ca ions in the SBF solution are involved in corrosion reaction and incorporated corrosion precipitants formed onto the samples.

3.6 In vitro activity of films against *S. aureus*

The antibacterial efficacies of the bare and coated Mg alloy against *S. aureus* bacteria were assessed by ZOI testing. The formation of a ZOI within a lawn of bacteria was used to evaluate the efficacy of released GS. A ZOI represents inhibition of the growth of an organism within a designated zone corresponding to the presence of an active substance. Figure 12 shows that after 24 h of incubation, the diameters of ZOI of the $(PSS/GS)_{20}$/Mg and $(PSS/GS)_{60}$/Mg are 18.68 and 23.98 mm, respectively, whereas there is no visible zone of inhibition for the uncoated Mg and NaOH-treated Mg. The good inhibition can be ascribed to the release of high dosage of diffusible GS from the multilayer coating into the surrounding medium. Based on these results, it can be concluded that LbL assembled coatings have significant antibacterial action on *S. aureus* bacteria and large number of assembled layers result in an obvious increase in antibacterial efficiency.

The antibacterial effect of the PSS/GS modified Mg alloy, evaluated by the plate-counting method is shown in Fig. 13. The CFUs of *S. aureus* decrease in the following order: $(PSS/GS)_{60}$/Mg > $(PSS/GS)_{20}$/Mg > AZ31 alloy > NaOH-treated Mg. Plating of a diluted sample from the control tube (the bare AZ31 alloy) yields 415 CFU. The sample treated with NaOH solution increases the CFU count to 612. Compared with NaOH-treated Mg, the bare Mg alloy shows better antibacterial activity, which can be ascribed to the fact that the corrosion products of Mg alloy would inhibit the

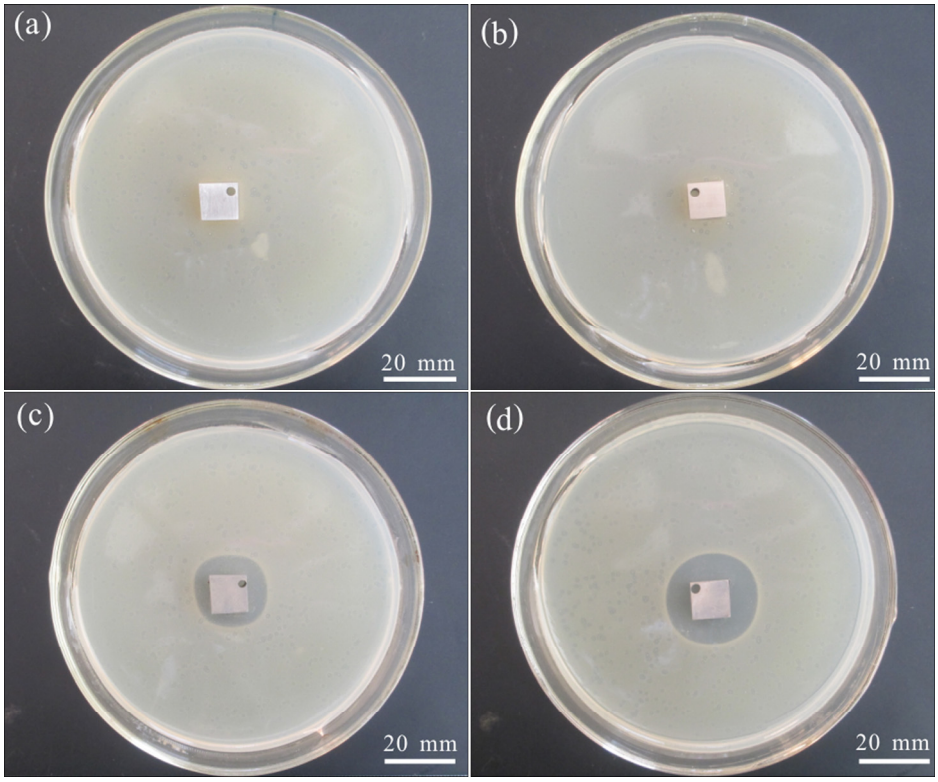

Fig. 12 ZOI of AZ31 alloy (a), NaOH-treated Mg (b), $(PSS/GS)_{20}$/Mg (c) and $(PSS/GS)_{60}$/Mg (d) samples against *S. aureus*

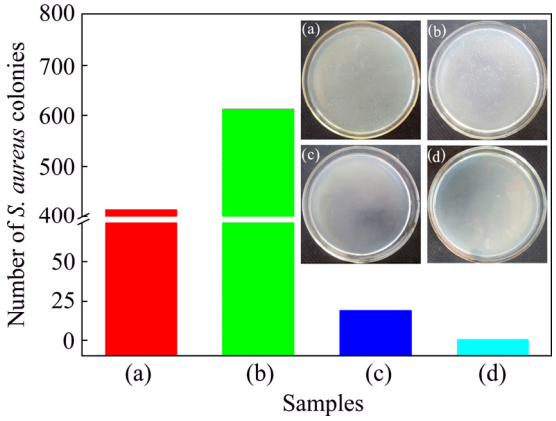

Fig. 13 Number of *S. aureus* colonies in antibacterial test (The inserted photographs of agar plates incubated under condition in the samples of AZ31 alloy (a), NaOH-treated Mg (b), $(PSS/GS)_{20}$/Mg (c) and $(PSS/GS)_{60}$/Mg (d))

growth of *S. aureus* [45]. Further modification with 20 bilayers of PSS/GS is able to reduce the CFU to 18, suggesting at least 96% reduction in bacteria viability. When the surface is coated with a number of 60 bilayers, the reduction rate of bacteria is approximately 100% after 2 h of incubation. This demonstrates that the antibacterial performance is greatly improved by increasing the number of bilayers, which is in accordance with the results of ZOI testing. What's more, as the high CFU levels applied in this study are rarely found in real-life systems, it appears that the LbL coating possesses an excellent biocidal effect and exhibits effectiveness in reducing bacteria growth.

4 Conclusions

1) Compared with bare AZ31 alloy, the $(PSS/GS)_n$/Mg samples exhibit both an improved corrosion resistance and excellent antibacterial property. The assembled multilayers are more effective in inhibiting the in *vitro* growth of *S. aureus* when the number of assembly is increased.

2) The data imply that there is probably an interaction between the $Mg(OH)_2$ film matrix and the polymer coatings, which undermines the corrosion resistance of the sample. The quality of the coating needs a further improvement.

References

[1] FEKRY A M, GHONEIM A A, AMEER M A. Electrochemical impedance spectroscopy of chitosan coated magnesium alloys in a synthetic sweat medium [J]. Surface and Coatings Technology, 2014, 238: 126−132.

[2] WITTE F. The history of biodegradable magnesium implants: A review [J]. Acta Biomaterialia, 2010, 6: 1680−1692.

[3] REN Ling, LIN-Xiao, TAN Li-li, YANG Ke. Effect of surface coating on antibacterial behavior of magnesium based metals [J]. Materials Letters, 2011, 65: 3509−3511.

[4] CHU Cheng-lin, HAN Xiao, BAI Jin, XUE Feng, CHU P K. Surface modification of biomedical magnesium alloy wires by micro-arc

oxidation [J]. Transactions of Nonferrous Metals Society of China, 2014, 24: 1058−1064.

[5] BERGE F, KRUGER L, OUAZIZ H, ULLRICH C. Influence of temperature and strain rate on flow stress behavior of twin-roll cast, rolled and heat-treated AZ31 magnesium alloys [J]. Transactions of Nonferrous Metals Society of China, 2015, 25(1): 1−13.

[6] ZHANG Fen, LIU Zhen-guo, ZENG Rong-chang, LI Shuo-qi, CUI Hong-zhi, SONG Liang, HAN En-hou. Corrosion resistance of Mg−Al−LDH coating on magnesium alloy AZ31 [J]. Surface and Coatings Technology, 2014, 258: 1152−1158.

[7] ZENG Rong-chang, SUN Xin-xin, SONG Ying-wei, ZHANG Fen, LI Shuo-qi, CUI Hong-zhi, HAN En-hou. Influence of solution temperature on corrosion resistance of Zn−Ca phosphate conversion coating on biomedical Mg−Li−Ca alloys [J]. Transactions of Nonferrous Metals Society of China, 2013, 23(11): 3293−3299.

[8] SEIFZADEH D, BEZAATPOUR A, ASADPOUR JOGHANI R. Corrosion inhibition effect of N, N'-bis (2-pyridylmethylidene)-1,2-diiminoethane on AZ91D magnesium alloy in acidic media [J]. Transactions of Nonferrous Metals Society of China, 2014, 24(11): 3441−3451.

[9] GUO Wei, WANG Qu-dong, YE Bing, ZHOU Hao, LIU Jian-feng. Microstructure and mechanical properties of AZ31−Mg_2Si in situ composite fabricated by repetitive upsetting [J]. Transactions of Nonferrous Metals Society of China, 2014, 24(12): 3755−3761.

[10] WONG S Y, MOSKOWITZ J S, VESELINOVIC J, ROSARIO R A, TIMACHOVA K, BLAISSE M R, FULLER R C, KLIBANOV A M, HAMMOND P T. Dual functional polyelectrolyte multilayer coatings for implants: Permanent microbicidal base with controlled release of therapeutic agents [J]. Journal of the American Chemical Society, 2010, 132: 17840−17848.

[11] CAO Hui-liang, LIU Xuan-yong, MENG Fan-hao, CHU P K. Biological actions of silver nanoparticles embedded in titanium controlled by micro-galvanic effects [J]. Biomaterials, 2011, 32: 693−705.

[12] LUO Peng, WANG Sheng-nan, ZHAO Ting-ting, LI Yan. Surface characteristics, corrosion behavior, and antibacterial property of Ag-implanted NiTi alloy [J]. Rare Metals, 2013, 32: 113−121.

[13] OSTROWSKI N, LEE B, ENICK N, CARLSON B, KUNJUKUNJU S, ROY A, KUNTA P N. Corrosion protection and improved cytocompatibility of biodegradable polymeric layer-by-layer coatings on AZ31 magnesium alloys [J]. Acta Biomaterialia, 2013, 9: 8704−8713.

[14] CHEN Liang, BROMBERG L, LEE J A, ZHANG Huan, SCHREUDER-GIBSON H, GIBSON P, WALKER J, HAMMOND P T, HATTON T A, RUTLEDGE G C. Multifunctional electrospun fabrics via layer-by-layer electrostatic assembly for chemical and biological protection [J]. Chemistry of Materials, 2010, 22: 1429−1436.

[15] DECHER G. Fuzzy nanoassemblies: Toward layered polymeric multicomposites [J]. Science, 1997, 277: 1232−1237.

[16] GOMES E C, OLIVEIRA M A S. Corrosion protection by multilayer coating using layer-by-layer technique [J]. Surface and Coatings Technology, 2011, 205: 2857−2864.

[17] SCHMIDT D J, MOSKOWITZ J S, HAMMOND P T. Electrically triggered release of a small molecule drug from a polyelectrolyte multilayer coating [J]. Chemistry of Materials, 2010, 22: 6416−6425.

[18] MIN J, BRAATZ R D, HAMMOND P T. Tunable staged release of therapeutics from layer-by-layer coatings with clay interlayer barrier [J]. Biomaterials, 2014, 35: 2507−2517.

[19] ZHU Yan-ying, WU Guang-ming, ZHANG Yun-hong, ZHAO Qing. Growth and characterization of $Mg(OH)_2$ film on magnesium alloy AZ31 [J]. Applied Surface Science, 2011, 257: 6129−6137.

[20] PICHAVANT L, AMADOR G, JACQUELINE C, BROUILLAUD B, HEROGUEZ V, DURRIEU M C. pH-controlled delivery of gentamicin sulfate from orthopedic devices preventing nosocomial infections [J]. Journal of Controlled Release, 2012, 162: 373−381.

[21] CICCO F D, REVERCHON E, ADAMI R, AURIEMMA G, RUSSO P, CALABRESE E C, PORTA A, AQUINO R P, GAUDIO P D. In situ forming antibacterial dextran blend hydrogel for wound dressing: SAA technology vs. spray drying [J]. Carbohydrate polymers, 2014, 101: 1216−1224.

[22] FENG Jing, CHEN Yan, LIU Xiao-han, LIU Tian-di, ZOU Lin-yi, WANG Yu-ting, REN Yue-ming, FAN Zhuang-jun, LV Yan-zhuo, ZHANG Mi-lin. In-situ hydrothermal crystallization $Mg(OH)_2$ films on magnesium alloy AZ91 and their corrosion resistance properties [J]. Materials Chemistry and Physics, 2013, 143: 322−329.

[23] ZHU Yan-ying, ZHAO Qing, ZHANG Yun-hong, WU Guang-ming. Hydrothermal synthesis of protective coating on magnesium alloy using de-ionized water [J]. Surface and Coatings Technology, 2012, 206: 2961−2966.

[24] KUNJUNKUNJU S, ROY A, RAMANATHAN M, LEE B, CANDIELLO J E, KUMTA P N. A layer-by-layer approach to natural polymer-derived bioactive coatings on magnesium alloys [J]. Acta Biomaterialia, 2013, 9: 8690−8703.

[25] TEYBALA A, SZYK-WARSZYNSKA L, WARSZYNSKI P. The effect of anchoring PEI layer on the build-up of polyelectrolyte multilayer films at homogeneous and heterogeneous surfaces [J]. Colloids and Surfaces A: Physicochemical and Engineering Aspects, 2009, 343: 127−132.

[26] ZENG Rong-chang, ZHANG Fen, LAN Zi-dong, CUI Hong-zhi, HAN En-hou. Corrosion resistance of calcium-modified zinc phosphate conversion coatings on magnesium-aluminium alloys [J]. Corrosion Science, 2014, 88: 452−459.

[27] SONG Cun-feng, CHANG Ying, CHENG Ling, XU Yi-ting, CHEN Xiao-ling, ZHANG Long, ZHONG Li-na, DAI Li-zong. Preparation, characterization, and antibacterial activity studies of silver-loaded poly(styrene-*co*-acrylic acid) nanocomposites [J]. Materials Science and Engineering C, 2014, 36: 146−151.

[28] CHAMAKURA K, PEREZ-BALLESTERO R, LUO Zhi-ping, BASHIR S, LIU Jing-bo. Comparison of bactericidal activities of silver nanoparticles with common chemical disinfectants [J]. Colloids and Surfaces B: Biointerfaces, 2011, 84: 88−96.

[29] ZENG Rong-chang, LAN Zi-dong, KONG Ling-hong, HUANG Yuan-ding, CUI Hong-zhi. Characterization of calcium-modified zinc phosphate conversion coatings and their influences on corrosion resistance of AZ31 alloy [J]. Surface and Coatings Technology, 2011, 205: 3347−3355.

[30] GRAY J E, LUAN B. Protective coatings on magnesium and its alloys—A critical review [J]. Journal of Alloys and Compounds, 2002, 336: 88−113.

[31] LIU Hui, YI Jian-hong. Polystyrene/magnesium hydroxide nanocomposite particles prepared by surface-initiated in-situ polymerization [J]. Applied Surface Science, 2009, 55: 5714−5720.

[32] YAN Hong, ZHANG Xue-hu, WEI Li-qiao, LIU Xu-guang, XU Bing-she. Hydrophobic magnesium hydroxide nanoparticles via oleic acid and poly(methyl methacrylate)-grafting surface modification [J]. Powder Technology, 2009, 193: 125−129.

[33] XIN Yun-chang, HUO Kai-fu, TAO Hu, TANG Guo-yi, CHU P K. Influence of aggresive ions on degradation behavior of biomedical magnesium alloy in physiological environment [J]. Acta Biomaterialia, 2008, 4: 2008−2015.

[34] CHEN Li, YUAN Chang-zhou, DOU Hui, GAO Bo, CHEN Sheng-yao, ZHANG Xiao-gang. Synthesis and electrochemical capacitance of core-shell poly (3,4-ethylenedioxythiophene)/poly (sodium 4-styrenesulfonate)-modified multiwalled carbon nanotube nanocomposites [J]. Electrochimica Acta, 2009, 54: 2335−2341.

[35] NASEF M M, SAIDI H, DAHLAN K Z M. Kinetic investigations of graft copolymerization of sodium styrene sulfonate onto electron

beam irradiated poly(vinylidene fluoride) films [J]. Radiation Physics and Chemistry, 2011, 80: 66−75.

[36] NAMPI P P, MOHAN V S, SINHA A K, VARMA H. High surface area sol−gel nano silica as a novel drug carrier substrate [J]. Materials Research Bulletin, 2012, 47: 1379−1384.

[37] LIU Peng, PAN Xin, YANG Wei-hu, CAI Kai-yong, CHEN Ya-shao. Improved anticorrosion of magnesium alloy via layer-by-layer self-assembly technique combined with micro-arc oxidation [J]. Materials Letters, 2012, 75: 118−121.

[38] LIU X, YUE Z L, ROMEO T, WEBER J, SCHEUERMANN T, MOULTON S, WALLACE G. Biofunctionalized anti-corrosive silane coatings for magnesium alloys [J]. Acta Biomaterialia, 2013, 9: 8671−8677.

[39] ZOMORODIAN A, BRUSCIOTTI F, FERNANDES A, CARMEZIM M J, MOURAE SILVA T, FERNANDES J C S, MONTEMOR M F. Anti-corrosion performance of new silane coating for corrosion protection of AZ31 magnesium alloy in Hank's solution [J]. Surface and Coatings Technology, 2012, 206: 4368−4375.

[40] ZHOU Wan-qiu, SHAN Da-yong, HAN En-hou, KE Wei. Comparison in characterization of composite and sol-gel coating on AZ31 magnesium alloy [J]. Transactions of Nonferrous Metals Society of China, 2010, 20(S2): s665−s669.

[41] ZHANG Rui-yue, CAI Shu, XU Guo-hua, ZHAO Huan, LI Yan, WANG Xue-xin, HUANG Kai, REN Meng-guo, WU Xiao-dong. Crack self-healing of phytic acid conversion coating on AZ31 magnesium alloy by heat treatment and the corrosion resistance [J]. Applied Surface Science, 2014, 313: 896−904.

[42] ZENG Rong-chang, QI Wei-chen, SONG Ying-wei, HE Qing-kun, CUI Hong-zhi, HAN En-hou. In vitro degradation of MAO/PLA coating on Mg−1.21Li−1.12Ca−1.0Y alloy [J]. Frontiers of Materials Science, 2014, 8: 343−353.

[43] FEKRY A M, EL-SHEERIF R M. Electrochemical corrosion behavior of magnesium and titanium alloys in simulated body fluid [J]. Electrochimica Acta, 2009, 54: 7280−7285.

[44] XIN Yun-chang, HUO Kai-fu, TAO Hu, TANG Guo-yi, CHU P K. Influence of aggressive ions on the degradation behavior of biomedical magnesium alloy in physiological environment [J]. Acta Biomaterialia, 2008, 4: 2008−2015.

[45] ROBINSON D A, GRIFFITH R W, SHECHTMAN D, EVANS R B, CONZEMIUS M G. In vitro antibacterial properties of magnesium metal against *Escherichia coli*, *Pseudomonas aeruginosa* and *Staphylococcus aureus* [J]. Acta Biomaterialia, 2010, 6: 1869−1877.

AZ31 镁合金表面层层组装 PSS/GS 膜的体外耐蚀与抗菌性能

曾荣昌[1,2]，刘丽君[1]，骆凯捷[1]，沈 俐[1]，张 芬[1]，李硕琦[1]，邹玉红[3]

1. 山东科技大学 材料科学与工程学院，青岛 266590；
2. 山东科技大学 矿山灾害预防控制省部共建国家重点实验室培育基地，青岛 266590；
3. 山东科技大学 化学与环境工程学院，青岛 266590

摘 要：为提高镁合金的耐蚀性，并且使其表面具有抗菌功能，从而抑制生物膜的形成和生物腐蚀，利用原位水热法在 AZ31 镁合金基体上制备氢氧化镁膜以及层层组装制备硫酸庆大霉素(GS)和聚苯乙烯磺酸钠(PSS)多层膜。利用扫描电子显微镜、傅里叶红外光谱、X 射线光电子能谱、电化学测试和浸泡实验研究$(PSS/GS)_n$Mg 复合膜层的表面形貌、化学成分和耐腐蚀性能。最后，通过抑菌圈实验和平板计数法评定$(PSS/GS)_n$Mg 样品抵抗金黄葡萄球菌的性能。结果表明，在镁合金表面制备的复合膜层表现出较好的耐蚀和抗菌性能。这种复合膜层可用作医疗植入器件涂层。

关键词：镁合金；耐蚀；抗菌性能；层层组装

(Edited by Xiang-qun LI)